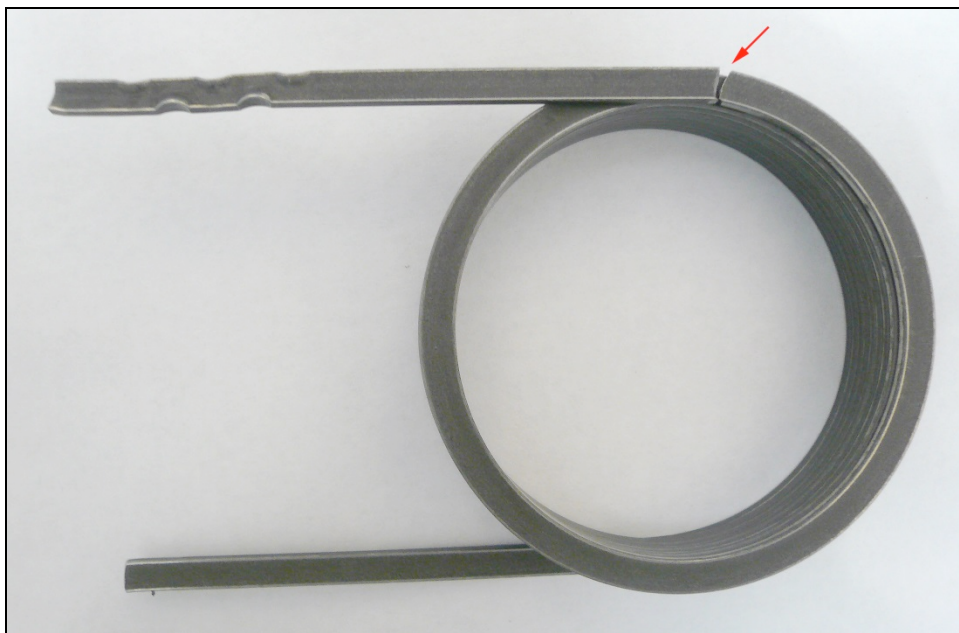


RTI PAST PERFORMANCE		
RTI Tracking Number:	1408703	8/18/2014
Core Task:	Chemical Analysis , Metallurgical Testing	
Analytical Techniques	Chem/Feature/Microhardness/SEM/Photo	

### **Metallographic observations:**

The failed during testing clutch spring was received for analysis (See Fig 1). The target of the analysis was to investigate the nature of the failure by using a variety of the metallographic techniques. It should be noted that adjacent components were made available for the submitted spring. The results of the analyses are provided below.



As-received for analysis.

Figure 1.

Enlarged size.

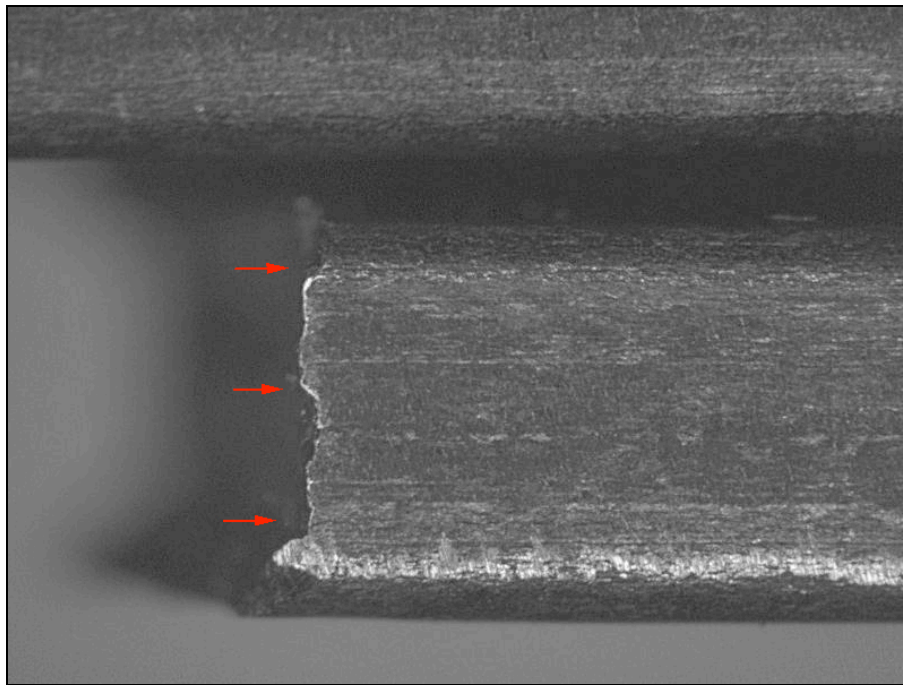
Red arrow points to the fractured region.

### **Macro Examination / Fractography.**

Macro examination, both visual and under a low power microscope has revealed a series of conditions as follows:

1. Location of the fracture suggests that the part is exposed to the highest stress at the beginning of the first revolution of the spring during service.
2. Examination of the fractured surfaces at low power magnification revealed that the fracture originated at the top (O.D.) surface of the spring coil. The top of the fracture propagated in a straight line - perpendicular to the rolling direction of the spring wire. There is no evidence of any surface defects such as seam, pits, die marks and other defects tending to impair the use the spring wire associated with fracture origins (see fig.2).

3. Examination of the fractured surfaces at low power magnification also revealed that the bottom (I.D.) surface of the spring coil at the fractured region has evidence of severe abrasive material wear due to metal-to-metal contact with supporting member (See fig.3). It should be noted that the severe material wear will cause reduction of the cross-section area and respectively decreases the ultimate strength to the cyclical loading. Also, changing in cross-section geometry of the spring will inflect angle of the bending during the service and respectively increases stress at the top (O.D) tension side of the spring.
4. The outer side of the second revolution of the spring coil revealed rubbing mark at the region adjacent to the fracture (see fig.4), which indicate presence of misalignment between spring and adjacent members.
5. Macro-examination of the fractured faces at both sides revealed that the fracture-cracks originated at multiple points along the top (tension side) of the spring and propagated at an angle toward the center region of the cross-section where catastrophic final fracture occurred (Note: shear lip visible at all three side.). The offset of the origin of the fracture at the top (O.D.) side of the spring indicates misalignment and respectively presence of some torsion loading (see fig. 5 and fig.6) during service. It should be noted that the fatigue morphologies at the origins of the fractures also observed (see fig. 7).

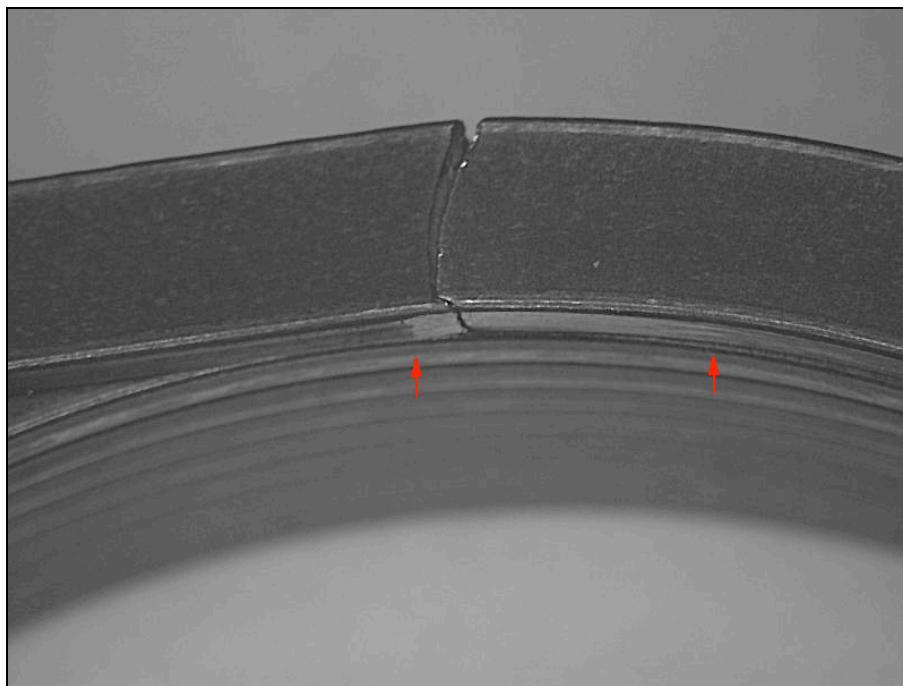


As-received for analysis.

Figure 2.

40x.

Macro-image illustrates surface condition at the top (O.D) surface of the spring coil near the fractured region. Red arrows point to the fractured region.

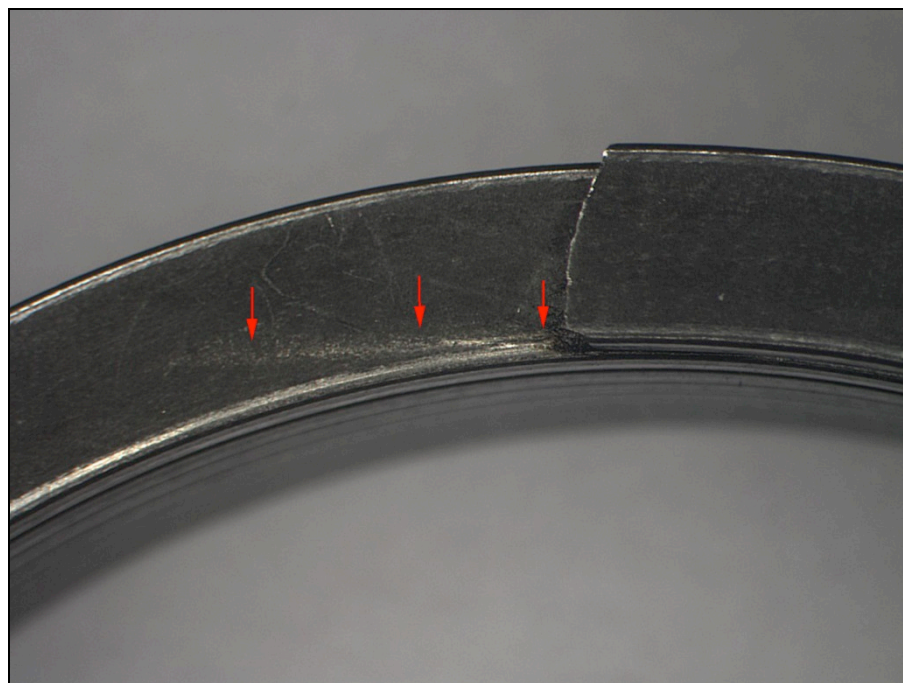


As-received for analysis.

Figure 3.

8x.

Macro-image illustrates severe abrasive material wear at the bottom (I.D.) surface of the spring near the fractured region. Red arrows point to the worn region.

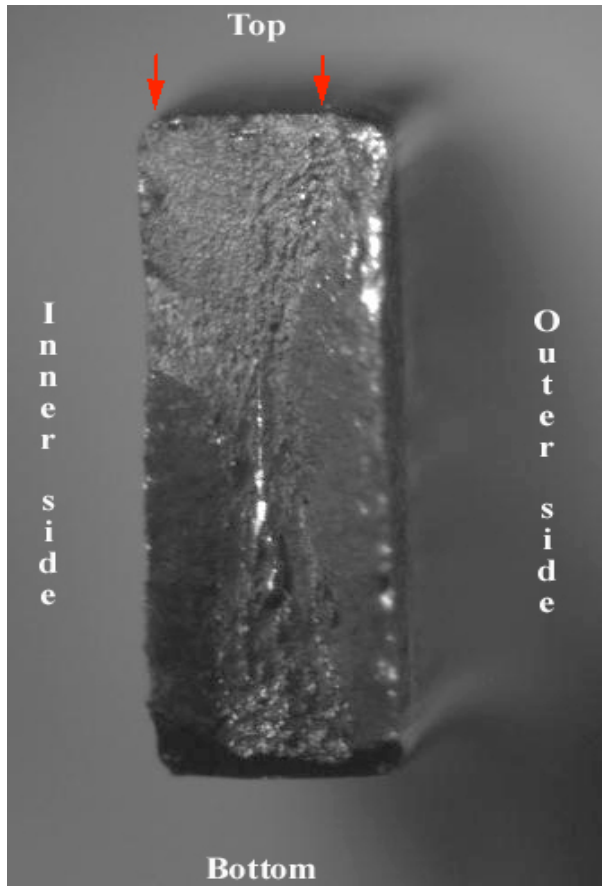


As-received for analysis.

Figure 4.

7x.

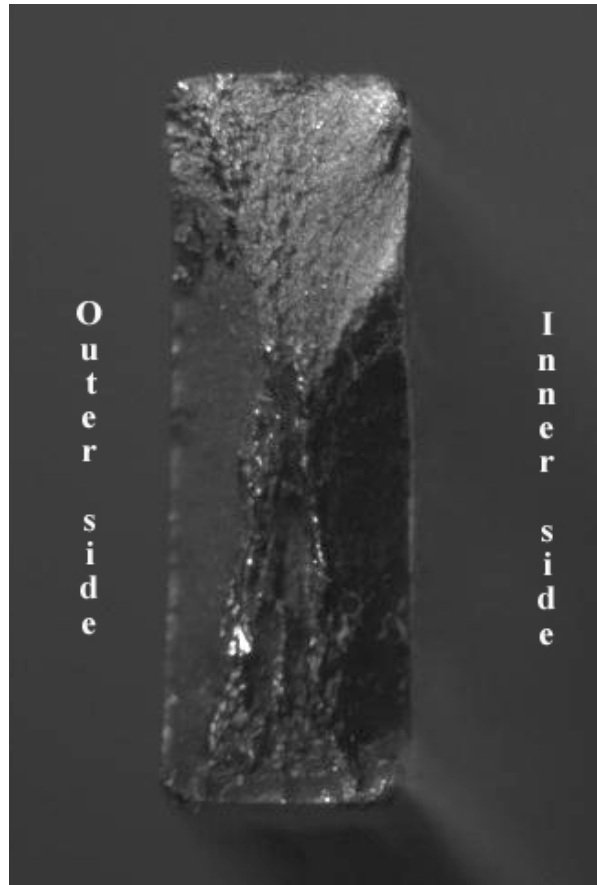
Macro-image illustrates rubbing mark at the outer side of the second revolution of the spring coil.



One side

Figure 5

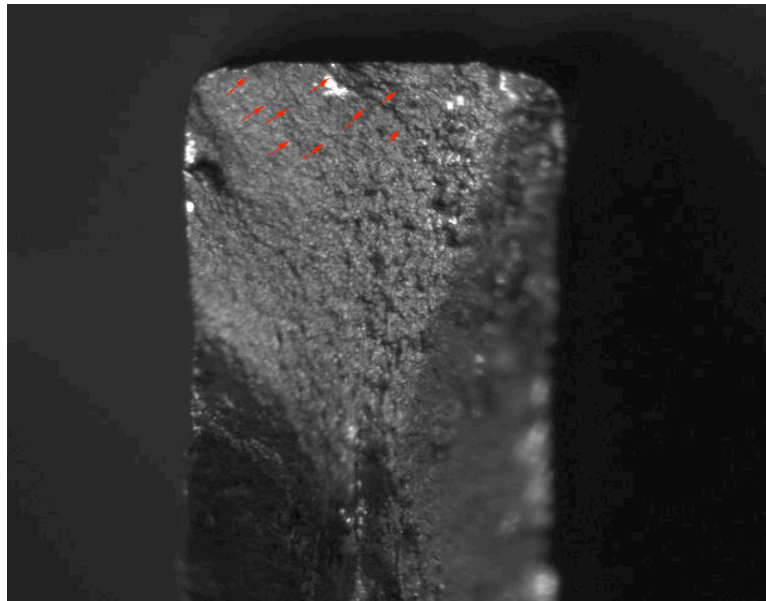
20x



Opposite side

Figure 6

22x



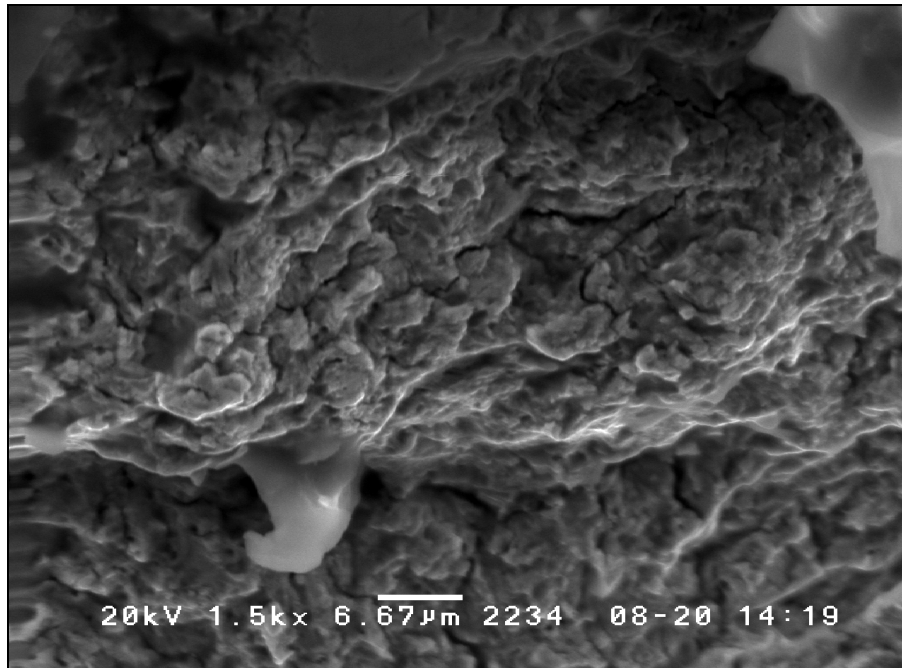
As-received for analysis.

Figure 7.

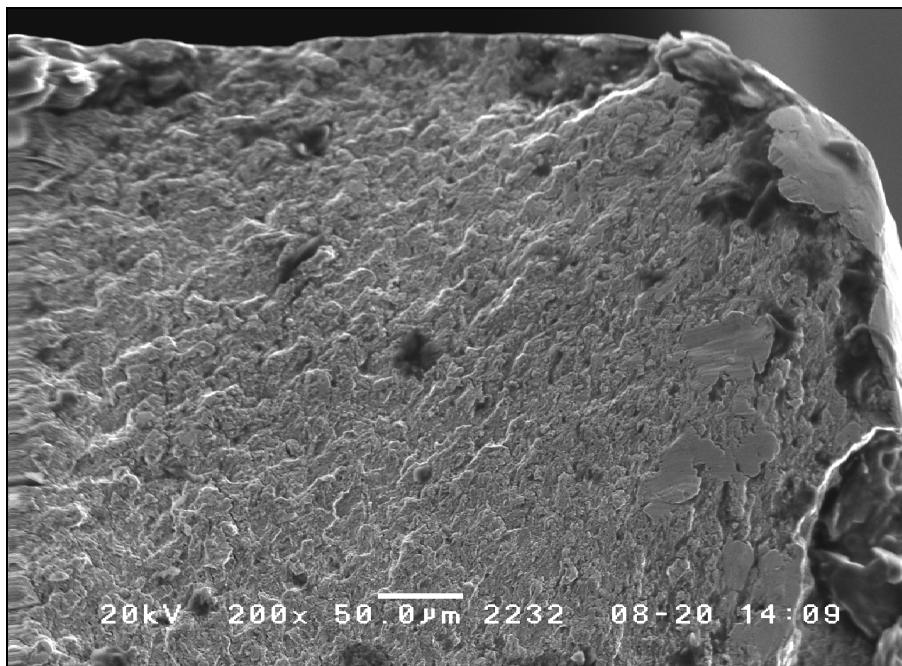
40x.

Red arrows point to fatigue morphologies.

Detailed examination of the fracture surface by SEM revealed multiple-origins of fatigue cracks at the top (O.D. surface) surface of the spring wire, which extended almost through the cross-section before final rupture occurred (see fig. 8 & fig.9).



SEM Figure 8. 1500x  
SEM image illustrates fatigue morphologies at the top surface of the spring wire.



SEM Figure 9. 200x  
SEM image illustrates fatigue morphologies extended almost through the cross-section before final rupture occurred.



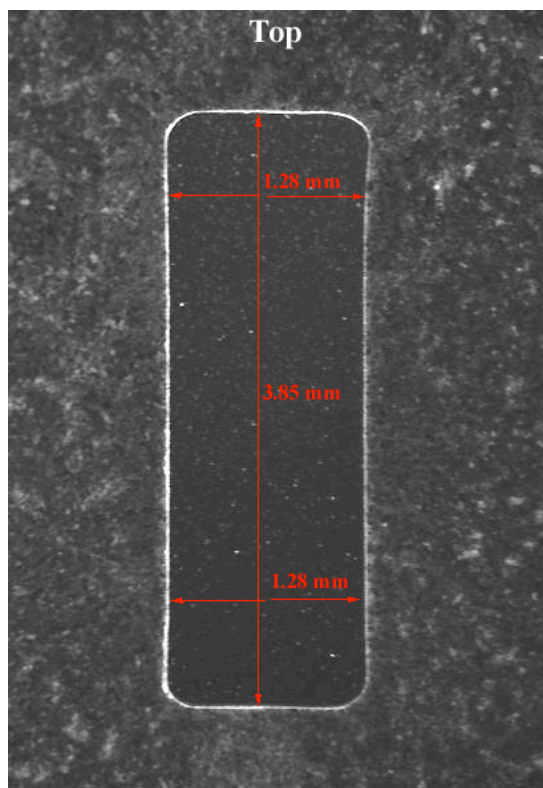
**Metallography:**

To further the investigation, the spring was sectioned transversally near the fractured side and longitudinally (along rolling direction), metallographically prepared in accordance with ASTM E3-11, and microscopically examined in the as-polished and etched conditions.

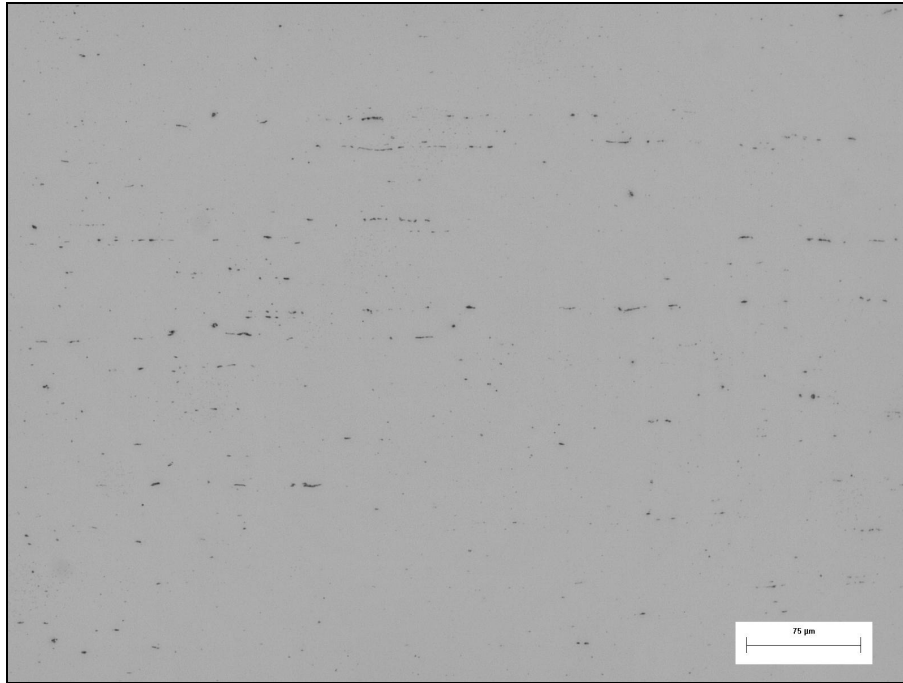
The transverse cross-section of the polished specimen illustrates the profile of the spring and dimensions (see fig.10). It should be noted that the spring actual dimensions is at the lower limit of blueprint requirement.

Metallographic examination of the as polished longitudinal cross-section revealed numerous linearly distributed plastically deformed non-metallic inclusions (see fig.11). The density and amount of the non-metallic inclusions is slightly above then typically observed.

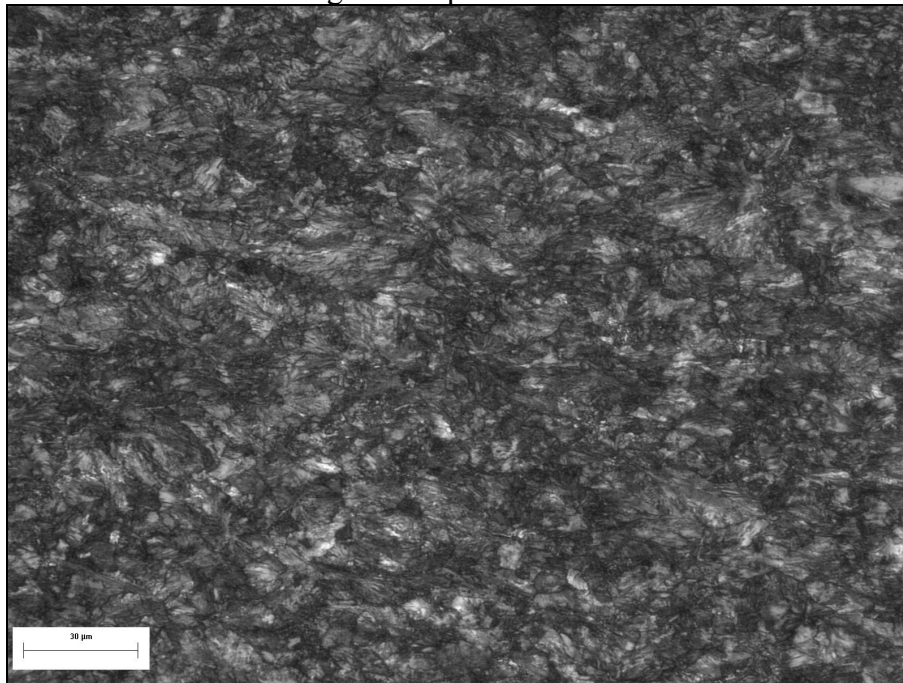
Metallographic examination of the longitudinal etched cross-section revealed a uniform microstructure throughout the matrix, which consists of what appears to be deformed pearlitic colonies (prior structure was very fine lamellar pearlite) (see fig.12).



As-polished condition. Figure 10. 20x  
Macro-image illustrates profile of the spring and dimensions.



As-polished condition. Figure 11. 200x  
Micro-image of a representative structure.



Etched with Nital. Figure 12. 500x  
Micro-image of a representative structure.

**Physical tests:** Analytical Method: ASTM E384-11<sup>e1</sup>

Micro-hardness indentations readings were taken on the transversally sectioned and mounted sample at the central area of cross-section using Vickers at 500 gram-force load and then converting to ROCKWELL "C" using ASTM E140-12be1 Table 7. The microhardness values, converted to the Rockwell C scale, are shown in table below. Please see the results of the hardness tests in Table 1 below.

**Table 1.**

Designation	Reading # 1		Reading # 2		Reading # 3		Reading # 4		Reading # 5	
	HV <sub>0.5</sub>	HRC	HV <sub>0.5</sub>	HRC	HV <sub>0.5</sub>	HRC	HV <sub>0.5</sub>	HRC	HV <sub>0.5</sub>	HRC
Spring	497.4	<b>49.0</b>	485.6	<b>48.1</b>	490.9	<b>48.5</b>	488.1	<b>48.3</b>	486.4	<b>48.9</b>

**Chemical Analysis:** Analytical methods:

ASTM E1019-11: Determination of Carbon, Sulfur, Nitrogen and Oxygen in Steel and Iron, Nickel, and Cobalt Alloys.

Instrument Operation of Perkin-Elmer Optima 30000 Inductively Coupled Plasma-Atomic Emission Spectrometer (ICP-AES).

The composition requirements for Music Spring wire ASTM A228 are also given for reference.

Designation	Elements (All units are wt-%)				
	C	S	P	Si	Mn
Analyzed Sample	0.83	0.013	<0.005	0.197	0.48
Specification limits for ASTM A228	0.70 min 1.00 max	0.030 max	0.025 max	0.10 min 0.30 max	0.20 min 0.60 max



**Conclusions:**

1. Metallographic analysis revealed that the wire was made from a good quality carbon steel material per ASTM A288. However, since no customer specifications indicating the exact hardness properties of the material were provided, the analysis cannot determine if the material will meet the desired application.

2. Fracture of the wire occurred by fatigue and originates at the top surface (O.D. surface of the spring coil). Microscopic examination of the longitudinal cross-section of the wire revealed that the cold forming of the material caused residual stresses that are favorable in the direction of forming (longitudinal dir.) and unfavorable in the opposite direction (transverse dir.). Therefore, the upper surface of the wire, which during cycle testing, is stretched in tension, is sensitive to the horizontal bending. The bottom (I.D.) surface of the spring coil at the fractured region has severe abrasive material wear, which changed cross-section area and inflect the angle of the bending. The bending load, which was applied during testing in the transverse direction, exceeded the strength of the wire at the worn region. It should be noted that the misalignment between spring and adjacent members also observed.

Note: The findings/opinions in this report are based on the analysis of the failed parts received and the information provided. If additional information becomes available, we reserve the right to supplement the findings of this report based on that information.

---

The data and information presented herein, while not guaranteed, are to the best of our knowledge accurate and true. No warranty or guarantee implied or expressed is made regarding these analytical results, since securing and properly preserving representative samples and since sample custody chains are beyond RTI control. The results provided by RTI are neither intended to suggest product merchantability, nor for use in infringement of any existing patent. RTI will not assume any liability or responsibility for any such infringement. Alteration or reproduction other than in its entirety is not authorized by RTI Laboratories, Inc. It is implied that some or all of the parameters reported herein are not covered by accreditation scope. Accreditation scope documents can be inspected at [www.rtilab.com](http://www.rtilab.com) or are available by request. A2LA certificate numbers 570.01 and 570.02. The recording of False, Fictitious or Fraudulent Statements or entry on this document may be punishable as a Felony under Federal Statute. All testing performed under RTI quality manual 1-QAO-001 rev L issued Dec. 2008 and has been audited and deemed compliant to ISO Guide 17025 rev. 2005